

Quantum Interference between the Third and Fourth Exciton States in Semiconducting Carbon Nanotubes Using Resonance Raman Spectroscopy

Juan G. Duque,^{1,2} Hagen Telg,¹ Hang Chen,³ Anna K. Swan,³ Andrew P. Shreve,^{1,4} Xiaomin Tu,⁵ Ming Zheng,⁵ and Stephen K. Doorn^{1,*}

¹Center for Integrated Nanotechnologies, Los Alamos National Laboratory, Los Alamos, New Mexico 87545, USA

²Physical Chemistry and Applied Spectroscopy Group, Los Alamos National Laboratory, Los Alamos, New Mexico 87545, USA

³Department of Electrical and Computer Engineering, and Photonics Center, Boston University, Boston, Massachusetts 02215, USA

⁴Center for Biomedical Engineering and Department of Chemical and Nuclear Engineering, University of New Mexico, Albuquerque, New Mexico 87131, USA

⁵Polymers Division, National Institute of Standards and Technology, 100 Bureau Drive, Gaithersburg, Maryland 20899-8540, USA

(Received 19 September 2011; published 16 March 2012)

We exploit an energy level crossover effect [Haroz *et al.*, *Phys. Rev. B* **77**, 125405 (2008)] to probe quantum interference in the resonance Raman response from carbon nanotube samples highly enriched in the single semiconducting chiralities of (8,6), (9,4), and (10,5). UV Raman excitation profiles of *G*-band spectra reveal unambiguous signatures of interference between the third and fourth excitonic states (E_{33} and E_{44}). Both constructive and destructive responses are observed and lead to anomalous intensity ratios in the LO and TO modes. Especially large anomalies for the (10,5) structure result from nearly identical energies found for the two E_{ii} transitions. The interference patterns demonstrate that the sign of the exciton-phonon coupling matrix elements changes for the LO mode between the two electronic states, and remains the same for the TO mode. Significant non-Condon contributions to the Raman response are also found.

DOI: [10.1103/PhysRevLett.108.117404](https://doi.org/10.1103/PhysRevLett.108.117404)

PACS numbers: 78.67.Ch, 73.22.-f, 78.30.Na

Single-wall carbon nanotubes (SWCNTs) serve as model 1D systems for studying distinctive electronic and optical phenomena, including ballistic transport, the Kohn anomaly, the Aharonov-Bohm effect, and exciton physics [1]. Their narrow, intense, excitonic transitions also make them nearly ideal for exploring another important optical behavior: quantum interference in the Raman response from closely spaced electronic states [2,3], an important subset of interference as a more general wave concept for any coherent interaction. Raman interference in molecular and solid-state systems has been studied extensively, and has been used to reveal forbidden transitions and hidden nonresonant behavior [4–7]. Often, however, broad spectra and measurement of low-frequency phonons prevent resolution of the relevant interfering resonances. Furthermore, spacing of interfering states is not readily tuned, limiting detailed study of the effect. SWCNTs, however, provide both structurally tunable transition energies [1] and access to high frequency modes for study. Theoretical recognition of the potential for interference effects in SWCNTs [8] has provided a basis for detailed analysis and attempts at direct measurement of interference via Raman excitation profiling on single tubes [9]. However, these results likely suffer from uncertainty in assignment of structural (n , m) indices and samples that probably occur as small bundles. Additionally, the possibility of interference between closely spaced upper and lower branches of metallic SWCNTs [10] has been inferred from indirect measurements [11]. Modeling of potential interference effects over multiple SWCNT structures has also been presented [12].

Interference in SWCNTs represents the phenomenon for very distinct points in the graphene k space. Interference phenomena in graphene itself has only recently been demonstrated via blocking of Raman *G*-mode interference pathways by electrostatic gating [13].

In semiconducting SWCNTs, interference becomes a possibility with resonance excitation into the third and fourth excitonic levels (E_{33} and E_{44}). For small-diameter mod 2 structures ($n-m:\text{mod}3 = 2$), the energies of these two states can approach closely and even cross over for certain chiralities [14,15], potentially leading to pronounced Raman interference effects. A clear demonstration of interference at the ensemble level requires resonance Raman excitation profiles (REPs) obtained from samples that are highly enriched in single chiralities, in order to avoid overlapping spectral response from other species. By acquiring REPs of the E_{33} and E_{44} transitions for the (8,6), (9,4), and (10,5) chiralities, we show here unambiguous evidence of quantum interference in the Raman response of the LO and TO *G*-band modes, which can lead to anomalous LO and TO intensity ratios. Furthermore, the relative signs of the LO matrix elements are found to reverse for the two transitions, while they remain the same for the TO mode. For the chiralities studied, systematic variation of E_{ii} energies with tube structure allows us to observe a range of interference effects as a function of energy separation between the interfering transitions. Analysis of the REPs also reveals evidence that recently discovered asymmetric responses

arising from non-Condon activity [16] are significant in these transitions as well.

Resonance Raman spectroscopy is performed on separate samples that have been highly enriched ($> 95\%$) in the (8,6), (9,4), and (10,5) mod 2 semiconductor chiralities via the previously reported DNA-based ion-exchange chromatography [17]. Following separation, SWCNTs in each sample are dialyzed into deoxycholate. Absorption spectra covering the second, third, and fourth excitonic transitions are shown in Fig. 1(a). For (8,6) and (9,4), the E_{33} and E_{44} transitions are well resolved. We note that the energy ordering of the third and fourth transitions is reversed for (9,4) [15]. For (10,5) the two transitions overlap and are not resolved. Extended tight binding calculations predict the (10,5) E_{33} and E_{44} to be within 50 meV of each other [18].

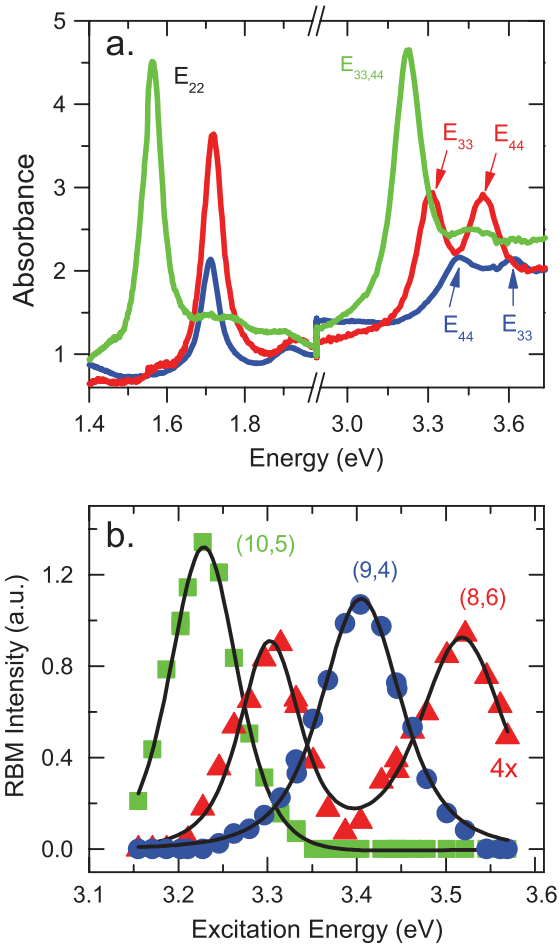


FIG. 1 (color). (a) Absorbance spectra of second, third, and fourth exciton transitions for (8,6) (red, $E_{33} = 3.31$ eV, $E_{44} = 3.50$ eV), (9,4) (blue, $E_{44} = 3.42$ eV, $E_{33} = 3.62$ eV), and (10,5) (green, $E_{33,44} = 3.22$ eV) SWCNT structures. (b) RBM REPs of third and fourth exciton transitions for (8,6) (red triangles), (9,4) (blue circles), and (10,5) (green squares) structures. Symbols: experimental data. Solid line: fit to data using Eq. (1) [19], with resulting E_{ii} of 3.30 and 3.49 eV [E_{33} and E_{44} for (8,6)], 3.39 eV [E_{44} for (9,4)], and 3.21 eV [E_{33} and E_{44} for (10,5)].

The intensity of the (10,5) E_{33}/E_{44} feature also nears that of the E_{22} [in comparison to the roughly half intensity shown for the individual (8,6) and (9,4) features], further suggesting the two transitions are nearly equal in energy for (10,5). For all three chiralities, energy separations of E_{33} and E_{44} are on the order of, or less than, the G -band energy (~ 197 meV), suggesting significant Raman interference effects might be expected.

Radial breathing mode (RBM) and G -band Raman spectra were obtained with 20 mW of excitation ranging from 2.92 to 3.58 eV, obtained by frequency doubling a cw Ti:sapphire laser in beta barium borate (BBO). Spectra were collected with 2 to 5 min integration times with a CCD after dispersion through a triple monochromator. Intensities of all spectra were corrected for instrument response using benzonitrile as an intensity and frequency reference [16]. RBM REPs [Fig. 1(b)] show clear E_{33} and E_{44} responses for (8,6), while the higher energy feature for (9,4) is not experimentally accessible. The single peak in the (10,5) REP further suggests the two transitions are closely spaced for this species. The E_{ii} values obtained from the RBM REPs are a close match to the absorbance maxima. The REPs are fit using Eq. (1), in which Raman

$$I_{\text{RRS}} \propto \left| A * \left[\frac{M_1^{33}}{E_L - E_{33} - i\frac{\Gamma_{33}}{2}} + \frac{M_2^{33}}{E_L - E_{33} - E_{\text{ph}} - i\frac{\Gamma_{33}}{2}} \right] + B * \left[\frac{M_1^{44}}{E_L - E_{44} - i\frac{\Gamma_{44}}{2}} + \frac{M_2^{44}}{E_L - E_{44} - E_{\text{ph}} - i\frac{\Gamma_{44}}{2}} \right] \right|^2 \quad (1)$$

intensity (I_{RRS}) depends on excitation, transition, and phonon energies (E_L , E_{ii} , E_{ph} , respectively) and a damping term Γ . Because the relative signs of contributions from E_{33} and E_{44} can differ in Eq. (1), summing all terms before squaring can result in constructive or destructive combination to introduce quantum interference. Conversely, non-interacting states may be represented in Eq. (1) by instead first squaring the bracketed terms for each E_{ii} , then summing. A and B represent the square of the absorbance matrix elements for the two transitions. The exciton-phonon coupling matrix elements for resonance with incident and scattered photons (so-called ingoing and outgoing resonances), respectively, are M_1^{ii} and M_2^{ii} . The relation $M_2/M_1 = -(1 - C)/(1 + C)$ is used to introduce non-Condon effects, where C gives the relative strength of non-Condon contributions [16]. We note in the absence of non-Condon effects ($C = 0$) that $M_1^{ii} = -M_2^{ii}$ [16]. For the fits in Fig. 1(b), E_{ph} is fixed to the observed RBM frequency, while the other parameters are adjustable [19].

E_{33} and E_{44} REPs for the G^+ (LO at 1590 cm^{-1}) and G^- (TO at 1551 cm^{-1}) modes of the (8,6) and (9,4) chiralities are shown in Fig. 2. In fitting the G -band REPs, E_{ph} is again fixed at the observed values and where possible the E_{ii} and Γ values are fixed at those found from the RBM REP fits, with the remaining parameters being adjustable [19]. We show

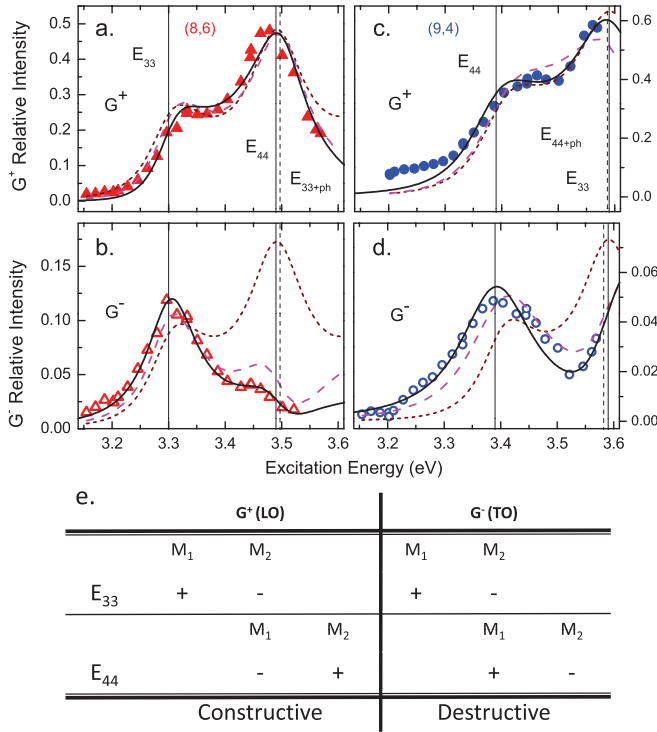


FIG. 2 (color). (a) and (b) (8,6) G^+ and G^- REPs, respectively. (c) and (d) (9,4) G^+ and G^- REPs, respectively. Symbols: experimental data. Red dotted line: model excluding interference and non-Condon effects. Magenta dashed line: fit including interference effects, $C = 0$. Black line: fit including interference and non-Condon effects [19]. Solid vertical lines designate E_{ii} positions (ingoing resonances), while vertical dashed lines designate positions of $E_{ii} + \text{phonon}$ energies (outgoing resonances). (e) Depiction of how relative sign of exciton-phonon coupling elements changes for G^+ vs G^- on going from E_{33} to E_{44} excitation. Horizontal position of signs represents relative alignment of relevant ingoing and outgoing resonances.

modeling for three limiting cases overlaid on the experimental data. Inspection of Fig. 2 for the first case shows that an assumption of noninteracting states with no non-Condon effects ($C = 0$) qualitatively represents the LO mode behavior for both chiralities. However, it gives a poor quantitative fit and is unable to describe the more complex behavior of the TO mode [Figs. 2(b) and 2(d)]. Significant improvement is found in the second case for both the LO and TO modes, in which the E_{33} and E_{44} Raman responses are allowed to interfere. Finally, when both quantum interference and non-Condon effects are included, excellent quantitative agreement between the fits and data is found for both modes in both chiralities.

The fitting analysis demonstrates that both interference between E_{33} and E_{44} and non-Condon contributions to the Raman response must be accounted for in describing the G -band REPs. However, significant uncertainty is present in our non-Condon parameter (C) values because the fits are not fully constrained. This is due to excitations being limited to < 3.6 eV, which prevents full coverage of the entire REP energy window. Despite this limitation, we are

able to use the E_{ii} and Γ values from the RBM REPs and absorption spectra to help constrain the fits. The result is a clear demonstration that non-Condon effects are significant. Furthermore, the non-Condon parameters that we extract ($C \sim 0.1-0.5$) are in agreement with values found previously for E_{22} excitation [16].

Most importantly, the observed interference provides insight into how the exciton-phonon coupling processes change with E_{ii} . First, we note that, as seen in the modeling results [red dotted line, Fig. 2(a)–2(d)] and as confirmed experimentally (see Ref. [16]), in the absence of quantum interference the REP shapes for the LO and TO are expected to behave similarly across their resonance windows. Instead, we observe here very different intensity profiles on comparing the LO to TO behaviors. In the vicinity of where the outgoing resonance of the lower energy transition overlaps with the ingoing resonance of the higher state [at ~ 3.49 eV for (8,6) and ~ 3.58 eV for (9,4)] the LO mode shows a significant enhancement of intensity, while the TO is suppressed. This opposing behavior of the two modes is a clear signature of interference and arises as a consequence of the opposite way in which the signs of the exciton-phonon coupling matrix elements for the two modes vary on going from E_{33} to E_{44} . Good fits to the data can only be obtained if the relative signs of ingoing and outgoing resonances (M_1 and M_2 , respectively) for the LO mode are reversed between E_{33} and E_{44} . In contrast, they remain the same for the TO mode. These sign behaviors are depicted in Fig. 2(e). Because the E_{33} – E_{44} energy spacing is approximately equal to the G -phonon energy, the result is constructive interference for the LO mode and destructive interference in the TO mode. We note that this contrasting behavior in the matrix elements has been predicted previously [20,21]. It is only the significant quantum interference present in the (8,6) and (9,4) structures that has allowed us to reveal experimentally this aspect of exciton-phonon coupling here.

We find the contrasting interference behaviors can also lead to anomalous LO/TO intensity ratios, depending on where in the REP one excites. Examples of (8,6) G -band spectra obtained at different excitation energies are shown in Figs. 3(a)–3(c). The different exciton-phonon coupling behavior discussed above for the LO and TO leads to REPs that are effectively out of phase with each other [Figs. 2(a) and 2(b)]. The result is that, while high energy excitations [Fig. 3(c)] are found to give the typically expected G -band spectrum (TO intensity \ll LO), some excitations can lead to equal intensities [Fig. 3(a)]. Even more striking are the anomalous LO/TO ratios found for the (10,5) structure. Over nearly the entire excitation range [Figs. 3(d)–3(f) and Fig. 4(a)] TO intensities are found to be significantly stronger than or equal to those of the LO mode.

REPs for the (10,5) LO and TO modes at the overlapping E_{33} and E_{44} resonances are shown in Figs. 4(b) and 4(c), respectively. The LO REP differs significantly from those for the (8,6) and (9,4) structures, showing a weak and nearly featureless profile over most of the excitation range,

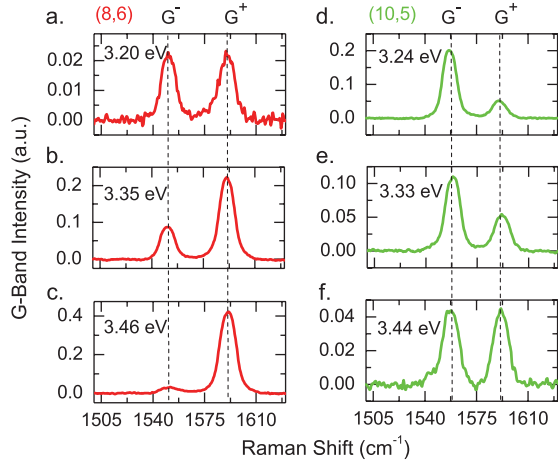


FIG. 3 (color). (8,6) G -band spectra obtained at excitation energies of (a) 3.20 eV, (b) 3.35 eV, and (c) 3.46 eV. (10,5) G -band spectra obtained at excitation energies of (d) 3.24 eV, (e) 3.33 eV, and (f) 3.44 eV. G -band spectra for all excitation energies are given as Supplemental Material [19].

and sits on a nonzero continuum background. Similar to the (8,6) and (9,4), however, the (10,5) TO REP shows an initial peak that drops to a lower intensity shoulder at higher energies.

Both the LO and TO REP features can be understood and modeled by applying the principles extracted from the (8,6) and (9,4) fits. One further consideration must be taken. As noted in the data of Fig. 1, the occurrence of a single spectral feature in both the absorbance spectrum and the RBM REP for the (10,5) suggests that its E_{33} and E_{44} transitions are nearly equal in energy. Given Γ values of ~ 120 meV, the two transitions would be visually resolved in the RBM REP at energy separations (ΔE_{33-44}) of 50 meV or greater. Thus, ΔE_{33-44} must be less than 50 meV. To test these principles, we first simulated LO and TO REPs using the relative behavior of the matrix elements from Fig. 2(e), applying a C value of 0.2, while varying ΔE_{33-44} . Within these constraints, when ΔE_{33-44} is about one G phonon of energy, the (8,6) and (9,4) REP features are recovered [19]. However, the main features of the (10,5) REPs cannot be reproduced unless ΔE_{33-44} is brought to 10 meV or less [19], further suggesting their energy separation must be small.

Applying these principles to fitting of the (10,5) REPs [using E_{ii} and Γ values extracted from the (10,5) absorbance and RBM data as starting points] results in excellent fits to the data. For the LO mode [Fig. 4(b)], a ΔE_{33-44} of ~ 1 meV [19] leads to nearly complete destructive interference, explaining the weak and featureless REP. That any LO intensity remains is likely due to differences in the magnitude of the E_{33} and E_{44} matrix elements. Non-Condon effects must also be included. However, while $C \sim 0.2$ is necessary to reproduce the data, its value is poorly constrained. We note the weak LO intensity also makes apparent a background contribution that may arise as a combination of nonresonant response plus

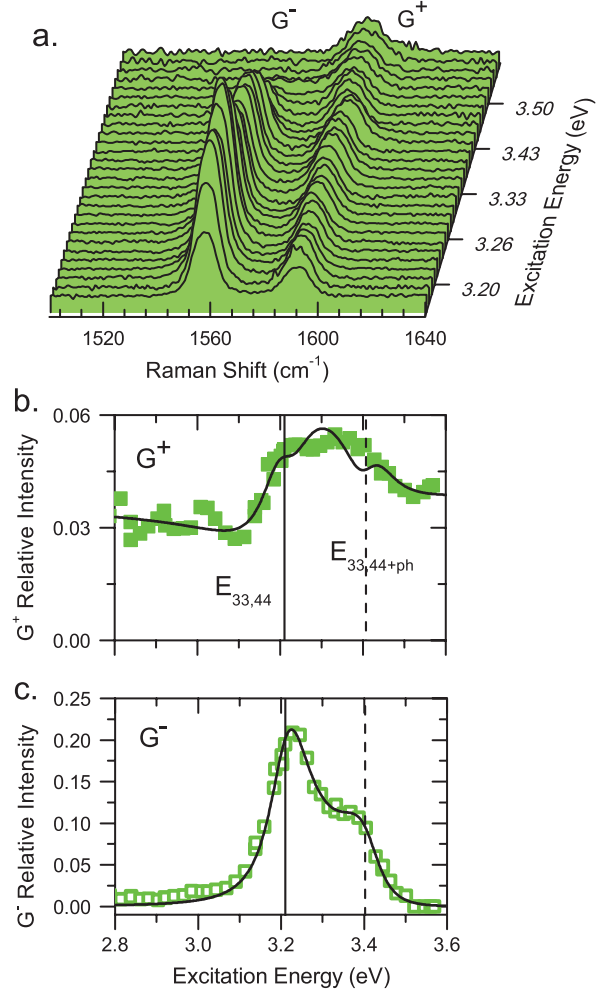


FIG. 4 (color). (10,5) G -band excitation behavior. (a) G -band spectra, excitation energy from 3.18 to 3.58 eV. (b) (10,5) G^+ (LO) REP, (c) (10,5) G^- (TO) REP. Symbols: experimental data. Solid lines: fit to Eq. (1) with $C = 0.22$ and continuum background included as $Ve^{i\theta}$ ($V = -0.19$ and $\theta = 0.066$) [19]. Solid vertical line designates $E_{33,44}$ position (ingoing resonance), while vertical dashed line designates position of $E_{33,44} +$ phonon energy (outgoing resonance).

contributions from overlapping E_{ii} continuum states [22]. We model these contributions by incorporating into Eq. (1) a constant term ($Ve^{i\theta}$, with $V = -0.19$ and $\theta = 0.066$) composed of real and imaginary parts, appropriate for describing combined nonresonant and continuum contributions over the limited excitation range of our experiment [19]. We note the fit in Fig. 4(b) is relatively insensitive to the value of the imaginary component (θ) [19].

The excellent fitting of the TO REP [Fig. 4(c)] also gives a ΔE_{33-44} of $\sim 1-2$ meV, consistent with the LO result. This condition results in strong constructive interference for the TO mode. The anomalous (10,5) LO/TO ratios shown in Figs. 3(d)–3(f) are thus understood as a result of the strongly opposing interference effects acting on the two modes. Because ΔE_{33-44} approaches zero, the asymmetry observed for the (10,5) TO REP is solely determined

by non-Condon effects, allowing an accurate determination of $C = 0.22 + / - 0.02$.

While extended tight binding calculations [18] predict a small (10,5) ΔE_{33-44} (~ 50 meV), the nearly 0 meV energy separation demonstrated here is a remarkable result. Whether this is a simple accident of electronic structure acted on by trigonal warping [15] or arises from additional unrecognized perturbations remains an open question for further study. Furthermore, with states so close in energy there may be unanticipated consequences for relaxation processes and pathways from excitations into this region for (10,5), providing motivation for performing dynamics measurements on this specific tube structure following excitation into E_{33} and E_{44} . Theoretical studies aimed at exploration of the possible consequences for other photophysical responses will also be of interest in this regard. The REP data also represent an ideal test system for modeling Raman response based on theoretical determination of the matrix elements for absorption [A and B, Eq. (1)] and exciton-phonon coupling (M_{ii}), Γ , and the recently revealed non-Condon effects (C) [16]. Additionally, the possibility of pairing the REPs with single-chirality absorption spectra makes the data well suited for modeling via Raman transform analysis [23,24] as an alternate to the sum-over-states approach used here [Eq. (1)].

In summary, through a judicious choice of specific chiral structures we have demonstrated unambiguously quantum interference effects in the Raman response from resonance excitation of closely spaced E_{33} and E_{44} transitions in mod 2 semiconducting SWCNTs. Such a clear demonstration results from a direct comparison of the global behaviors of the LO and TO modes across multiple tube structures. Observation of constructive and destructive interference effects are described self-consistently for each mode at the different energy spacings available with each structure. This ability allows extraction of the relative behavior of the signs of the Raman matrix elements, which can be important in determining a wide range of nonlinear optical responses and provides additional insight into the exciton-phonon coupling processes that underlie a tremendous range of nanotube photophysical behaviors. Additionally, our demonstration of quantum interference as the source of anomalous LO/TO intensity ratios may provide a mechanism for similarly observed behaviors commonly seen in single-tube Raman spectroscopy. Finally, our results demonstrate that non-Condon effects, only recently found to be important in the G-band Raman response in E_{22} excitation [16], must also be considered for the higher lying exciton transitions. These results also emphasize the importance of the availability of pure chirality samples for enabling the study of previously inaccessible optical behaviors in carbon nanotubes.

J. G. D., H. T., and S. K. D. acknowledge partial support from the LANL-LDRD program. A. P. S. acknowledges support from the U.S. Department of Energy, Office of Basic Energy Sciences. A. K. S. acknowledges NSF Grant

No. DMR-0706574. X. T. and M. Z. acknowledge NSF Grant No. CMS-060950. This work was performed in part at the Center for Integrated Nanotechnologies, a U.S. Department of Energy, Office of Basic Energy Sciences user facility.

*Author to whom all correspondence should be addressed.
skdoorn@lanl.gov

- [1] *Carbon Nanotubes: Advanced Topics in the Synthesis, Structure, Properties, and Applications*, Topics in Applied Physics Vol. 111, edited by A. Jorio, G. Dresselhaus, and M. S. Dresselhaus (Springer, Heidelberg, 2008).
- [2] M. Cardona, in *Light Scattering in Solids II*, edited by M. Cardona and G. Guntherodt, Topics in Applied Physics Vol. 50 (Springer, Heidelberg, 1982), Chap. 2, p. 19.
- [3] R. J. H. Clark and T. J. Dines, *Chem. Phys. Lett.* **79**, 321 (1981).
- [4] J. Menendez and M. Cardona, *Phys. Rev. B* **31**, 3696 (1985).
- [5] J. M. Ralston, R. L. Wadsack, and R. K. Chang, *Phys. Rev. Lett.* **25**, 814 (1970).
- [6] J. Friedman and R. M. Hochstrasser, *Chem. Phys. Lett.* **32**, 414 (1975).
- [7] P. Stein *et al.*, *J. Chem. Phys.* **64**, 2159 (1976).
- [8] M. Canonico *et al.*, *Phys. Rev. B* **65**, 201402(R) (2002).
- [9] G. Bussi, J. Menendez, J. Ren, M. Canonico, and E. Molinari, *Phys. Rev. B* **71**, 041404(R) (2005).
- [10] S. K. Doorn, P. T. Araujo, K. Hata, and A. Jorio, *Phys. Rev. B* **78**, 165408 (2008).
- [11] A. G. Souza Filho *et al.*, *Phys. Rev. Lett.* **95**, 217403 (2005).
- [12] J. Jiang *et al.*, *Phys. Rev. B* **71**, 205420 (2005).
- [13] C.-F. Chen *et al.*, *Nature (London)* **471**, 617 (2011).
- [14] K. Sato, R. Saito, J. Jiang, G. Dresselhaus, and M. S. Dresselhaus, *Phys. Rev. B* **76**, 195446 (2007).
- [15] E. H. Haroz, S. M. Bachilo, R. B. Weisman, and S. K. Doorn, *Phys. Rev. B* **77**, 125405 (2008).
- [16] J. G. Duque *et al.*, *ACS Nano* **5**, 5233 (2011).
- [17] X. Tu, S. Manohar, A. Jagota, and M. Zheng, *Nature (London)* **460**, 250 (2009).
- [18] Ge. G. Samsonidze *et al.*, *Appl. Phys. Lett.* **85**, 5703 (2004).
- [19] See Supplemental Material at <http://link.aps.org/supplemental/10.1103/PhysRevLett.108.117404> for all G-band spectra used in generating REPs, REP simulations as a function of ΔE_{ii} , a discussion of the sensitivity of the (10,5) fits to ΔE_{ii} , additional discussion of how continuum contributions are included in the (10,5) fitting, and tabulation of REP fitting parameters.
- [20] M. Machon, S. Reich, and C. Thomsen, *Phys. Rev. B* **74**, 205423 (2006).
- [21] V. N. Popov and P. Lambin, *Physica (Amsterdam)* **37E**, 97 (2007).
- [22] A. N. Vamivakas *et al.*, *Phys. Rev. B* **74**, 205405 (2006).
- [23] J. B. Page, in *Light Scattering in Solids VI*, edited by M. Cardona and G. Guntherodt, Topics in Applied Physics Vol. 68 (Springer, New York, 1991), Chap. 2, p. 17.
- [24] A. P. Shreve *et al.*, *Phys. Rev. Lett.* **98**, 037405 (2007).